Centrosomal Protein 55 increases chromosomal instability in ovarian cancer cells by controlling microtubule dynamics

Stefanie Muhs
University Medical Center Hamburg-Eppendorf
Simon A. Joosse
University Medical Center Hamburg-Eppendorf
Themistoklis Paraschiakos
University Medical Center Hamburg-Eppendorf
Paula Schäfer
University Medical Center Hamburg-Eppendorf
Sabine Windhorst (s.windhorst@uke.de)
University Medical Center Hamburg-Eppendorf

Research Article

Keywords:

Posted Date: May 23rd, 2022

DOI: https://doi.org/10.21203/rs.3.rs-1537124/v2

Abstract

Centrosomal Protein 55 (CEP55) exhibits different oncogenic activities; it regulates the PI3K-Akt-pathway, cellular abscission and chromosomal instability (CIN) in cancer cells. While the mechanism of CEP55-controlled PI3K-Akt signaling and cellular abscission are well-understood, its role in CIN has not been elucidated yet. Thus, the focus of this study was to address this issue. Depletion of CEP55 in ovarian cancer cells decreased the CIN rate, increased spindle microtubule-dynamics and decreased spindle microtubule-stability. In addition, recombinant CEP55 accelerated microtubule-polymerization and attenuated cold-induced microtubule-depolymerization. To analyze a potential relationship between CEP55 controlled CIN and its impact on microtubule-dynamics, the CEP55 microtubule-binding peptides were identified and a mutant with deficient microtubule-binding activity re-expressed in CEP55 depleted cells. This mutant did not restore decreased CIN in CEP55 depleted cells, indicating that CEP55 controls CIN by binding MTs. This knowledge now provides the possibility to selectively interfere with CEP55 controlled CIN in cancer cells.

Introduction

Ovarian cancer (OvCa) is the most lethal cancer among women and is treated by surgery and paclitaxel/cisplatin-based chemotherapy. Although initially the patients respond well to chemotherapy, most of them develop *chemo resistant* tumor populations due to their high adaptability to environmental stress(1). This adaptability is mainly caused by chromosomal instability (CIN) of OvCa cells(2). CIN is a cellular process describing chromosome segregation errors that result in aneuploidy in most cases(3). In CIN cells, chromosomes are not equally distributed to the daughter cells, leading to aneuploid cell populations with highly diverse chromosome numbers and selection of cells with the best-suited genome. This genomic plasticity leads to selection of cells adapted to environmental stress, like chemotherapy or changes of the microenvironment during the process of metastasis(4). Therefore, a high CIN score is associated with malignancy of tumor cells(5). Mechanistically, CIN results from defects of the DNA repair machinery or mis-regulation of microtubule spindle dynamics, resulting in misaligned chromosomes, chromosome mis-segregation and in formation of lagging chromosomes(6, 7). Lagging chromosomes can be embedded by membranes and establish as micronuclei (8).

The thymus and testis specific protein Centrosomal Protein 55 (CEP55) is overexpressed in many types of cancer, including ovarian cancer(9-11). CEP55 is a scaffold protein that binds to MTs *in vitro*(12) and is mainly located to the centrosome and the midbody(13, 14) , in the cytosol it shows a diffuse localization(13). It has been widely demonstrated that CEP55 overexpression in cancer cells correlates with bad prognosis(10) and CEP55 belongs to the CIN70 score in cancer patients(5). In accordance with these findings, overexpression of CEP55 in mice increased spontaneous tumorigenesis and the CIN rate in mouse embryonic fibroblasts (MEFs)(15).

In addition to its involvement in CIN, the protein has been shown to promote cellular abscission in Hela cells by recruiting the ESCRT proteins ALG-2-Interacting *Protein* X (Alix) and Tumor susceptibility gene

101 (TSG101) to the midbody(16). Furthermore, CEP55 stimulates the PI3K-Akt pathway by directly interacting with the regulatory p85 subunit of PI3K(17). However, how CEP55 controls CIN has not been elucidated yet.

In this study we addressed this question, and reveal that in OvCa cells CEP55 controls CIN by its MT-modulating activity. This finding now enables to selectively interfere with the CIN-promoting activity of CEP55.

Results

Depletion of CEP55 in OvCa cells reduces the speed of cellular abscission but does not affect the pAkt level

In order to analyze the oncogenic activities of CEP55 in OvCa cells, its mRNA was stably down-regulated via shRNA in two different OvCa cell lines with high CEP55 expression OVCAR-8 and SKOV-3. SKOV-3 sh1 and sh2 cells had a down-regulation efficiency of 83% and 66%, OVCAR-8 cells of 74% and 62% (Figure S1A). In addition, the specificity of CEP55 depletion was controlled by stably re-expressing the protein in CEP55 sh1 cells (Figure S1B).

Since CEP55 has been shown to control PI3K-Akt signaling, midbody separation and CIN, these cellular processes were compared between control and CEP55 manipulated cells. SKOV-3 and OVCAR-8 cells exhibited a high pAkt level even in non-stimulated cells, showing that in these cell lines Akt-signaling is constitutively activated. However, we did not find an effect of CEP55 depletion on the concentration of pAkt (Fig. 1A), indicating that in OvCa cells a high CEP55 level does not increase constitutively activated PI3K-Akt signaling.

On the other hand, measurement of midbody separation in SiR-tubulin-treated cells by life cell imaging revealed that strong and mild knock-down of CEP55 increased the time necessary for cellular abscission (Fig. 1B). To analyze whether this CEP55-controlled midbody separation was dependent on the CEP55-Alix interaction, a CEP55 mutant with deficient Alix-interaction was re-expressed in SKOV CEP55 sh1 cells ($CEP55^{Y187A}$). Thereby, we found that $CEP55^{Y187A}$ did not restore slowed cellular abscission of CEP55 depleted cells (Fig. 1C). Thus, also in OvCa cells a high CEP55 level accelerates the speed of cellular abscission in an Alix-dependent manner. However, although cellular division was decelerated in CEP55 depleted cells, no cleavage failures were detected as found in Hela cells (13) (data not shown) and hence no alterations of multinucleated cells (data not shown). Thus, a high CEP55 level accelerates cellular abscission in OvCa cells but is not necessary to complete this process.

In conclusion, in OvCa cells CEP55 does not control constitutively activated PI3K-Akt signaling but accelerates cytokinesis.

Depletion of CEP55 decreases CIN

The impact of CEP55 on CIN was analyzed by different assays. As first read out, the number of cells with properly aligned chromosomes (18) was compared between control and CEP55 shRNA cells. This evaluation revealed that strong down-regulation of CEP55 significantly increased the number of cells with aligned chromosomes, while moderate down-regulation had no significant effect (Fig. 2A). Re-expression of CEP55 reversed decreased misalignment in CEP55 shRNA cells, validating the specificity of the CEP55 knock-down effect (Fig. 2B). Likewise, the number of micronuclei, a consequence of lagging chromosomes(8), was reduced in sh1 cells, and this effect was rescued by re-expressing CEP55 (Fig. 1C).

Since chromosome misalignment can result in a higher diversity of chromosome number(3), chromosomes were counted in control and CEP55-manipulated cells (Fig. 2D, E). We found that the number of chromosomes was highly diverse in chromosomal instable scr control cells. This diversity was significantly decreased in sh1 but not in sh2 cells (Fig. 2D), and chromosome number was again highly diverse in cells re-expressing $CEP55^{WT}$ (Fig. 2E).

To further validate the role of CEP55 in genomic heterogeneity, whole genome, low coverage next generation sequencing of control and knock-down cells was performed. For evaluation of genomic heterogeneity, the median chromosome copy number of control cells was determined and this value was defined as baseline (bold black line in Fig. 3). Thereafter, the chromosome regions closer (green) or more distant (red) from this baseline in knock-down as compared to control cells was investigated. This calculation revealed that in knock-down cells a total of 481.5 Mbp were closer and 238.5 Mbp were more distant from baseline relative to control SKOV-3 cells. In OVCAR-8, 229.9 Mbp were closer and 162 Mbp were more distant. These results indicate that the heterogeneity of chromosomal aberrations within the ovarian cancer cell lines are reduced after knock-down of CEP55.

Together, the results from four different assays revealed that reduced CEP55 expression decreases CIN in OvCa cells.

CEP55 depletion reduces spindle MT-dynamics and increases spindle MT-stability

In contrast to the role of CEP55 in midbody separation, its function in CIN has not been elucidated yet(10). Therefore, the main focus of this study was to identify the CEP55 activity required for its CIN-inducing effect.

Since chromosomal misalignment can result from dysregulated spindle MT-dynamics(3) and CEP55 has been shown to directly bind to MTs *in vitro*(12), we analyzed whether CEP55 may be involved in the regulation of spindle MT-dynamics. For this, spindle MT-dynamics were compared between CEP55-manipulated cell lines from early to late metaphase. MTs were labeled with SiR-tubulin and spindle speed (µm/h) was assessed by life cell imaging with subsequent reconstruction of 3-D-images (for details, see methods). Calculation of spindle speed showed that, as expected, early metaphase spindle MTs were not motile, thus no differences were found between control and CEP55-manipulated cells. At late metaphase, however, the speed of spindle MTs increased 2.5-fold in CEP55 shRNA cells but only very weakly in

control cells as well as in shRNA cells re-expressing CEP55 (Fig. 4A-C). Thus, a high CEP55 level seems to reduce the speed of spindle MT dynamics.

In order to assess whether the alteration of MT-dynamics are associated with changed MT-stability, fixed M-phase cells were stained with antibodies against detyrosinated, thus stabilized MTs(19). The fraction of cells having stable or unstable cells was analyzed by counting cells with low centrosome signals (Fig. 4D, ”unstable”) and those with strong signals in centrosomes and in the spindle (Fig. 3D, ”stable”). This evaluation revealed that a strong CEP55 knock-down reduced the number of cells with stable spindle MTs.

In summary, our data show that down-regulation of CEP55 expression increases the speed and decreases stability of spindle MTs in metaphase cells.

Identification of CEP55 peptides required for MT-binding.

Our data show that CEP55 controls the CIN rate as well as spindle MT dynamics in OvCa cells. In order to reveal whether both findings are related, a CEP55 mutant with deleted MT-binding peptides has to be re-expressed in CEP55 sh1 cells and chromosome alignment and micronucleus formation assessed again. However, the CEP55 peptides required for MT-binding had not been identified yet and therefore this issue was addressed in this study.

Since MT-binding domains are not conserved in amino acid sequence or tertiary structure(20), we predicted the domain architecture of CEP55 using bioinformatics. CEP55 is a coiled-coil protein and so far, only the EABR domain has been characterized on a structural level(16). The secondary CEP55 structure mainly consists of α-helices, and coiled-coil (CC) domains, while β-sheets were only found in the C-terminal region (Figure S2). In addition, the 3-D structure of CEP55 was predicted by AlphaFold(21) (Fig. 5A, and Figure S3). Based on the coiled-coil predictions and the resolved EABR-Domain, we predicted CEP55 as a Dimer. In this model, the EABR domain is connected, N- and C-terminally, to large coiled-coil domains through loops, providing flexibility. The N- and C-termini are structured less complex with loops and short α-helices or ß-sheets. A leucine zipper-like structure seems to be formed, among which the N- and C-termini appear highly flexible.

On the basis of both predictions (Fig. 6A, S2, S3), functional segments were defined as indicated in Fig. 5B. Among these, we first deleted large N- and C-terminal segments (aa 1-126 and aa 362–464) or a large segment inside the protein (aa 127–361) (Fig. 6A). These truncation constructs were expressed in *E. coli* as His-GFP fusion proteins and enriched by nickel chelate chromatography (Fig. 6B). To analyze binding of His-GFP (control), full-length protein ($CEP55^{FL}$) and its mutants to MTs, three different methods were conducted. (1) Rhodamine labeled MTs were incubated with GFP-CEP55 fusion proteins and the localization of CEP55 proteins to MTs were analyzed by fluorescence microscopy (Fig. 6C). (2) CEP55 proteins were immobilized to GFP-dynabeads, the beads were incubated with MTs, and binding of MTs to CEP55 was analyzed by Western blotting (Fig. 6D). (3) An MT-pull down assay was performed and

binding of the CEP55 proteins to MTs was analyzed (Fig. 6E). Among these methods the last one enables to assess the strength of MT-binding as it is a ratiometric measurement.

All three methods showed that the full-length protein ($CEP55^{FL}$) bound to MTs while the $CEP55^{127–361}$ mutant did not. These data reveal that the MT-binding peptides reside in the N/C termini and assume that the $CEP55^{\Delta127–361}$ binds to the same extent to MTs as full-length CEP55 does. However, binding of $CEP55^{\Delta127–361}$ to MTs was reduced by 60% compared to full-length CEP55.

To further locate the N/C peptides required for MT-binding, the N-terminus (aa 1–58; $CEP55^{59–464}$), the C-terminus (aa 429–464; $CEP55^{1–428}$) and the N- and C-termini together ($CEP55^{59–428}$) were deleted (Fig. 7A) and assessed by the dynabeads assay. $CEP55^{1–428}$ and $CEP55^{59–464}$ showed an about 25% reduced, but not a deficient binding to MTs, while binding of $CEP55^{59428}$ to MTs was nearly completely abolished (> 90%) (Fig. 7B). This result was confirmed by the pull-down assay and by fluorescence microscopy (Fig. 7C, D). Thus, both the N- and the C-terminus are required for MT-binding. The isolated $CEP55^{\Delta59428}$, however, did not bind to MTs as assessed by fluorescence microscopy and by the pull-down assay. Since our AlphaFold prediction did not indicate strong intramolecular interactions (Fig. 8, Figure S3) of peptides inside $CEP55^{\Delta59428}$, masking the MT-binding sites, we conclude that full-length CEP55 is necessary to position the N/C-termini at MTs. Our finding that also $CEP55^{\Delta127–631}$ showed reduced MT-binding (Fig. 6E and 8) supports this conclusion.

Together, our data demonstrate that binding of CEP55 to MTs is mediated by the N- and the C-terminal peptides.

Re-expression of a MT-binding deficient CEP55 mutant does not rescue reduced CIN of CEP55 shRNA cells

The identification of the CEP55 peptides required for MT-binding has now enabled us to analyze the impact of CEP55 MT-binding on CIN. For this purpose, the N/C-terminus of CEP55 was deleted ($CEP55^{59428}$) and cloned into the lentiviral Lego vector. OVCAR-8 and SKOV-3 CEP55 shRNA cells were infected with the virus coding for $CEP55^{59428}$ and after selection of the cells expression of $CEP55^{59428}$ was validated by qPCR (Figure S4).

Before analyzing the impact of $CEP55^{59428}$ on CIN, we validated the relevance of the C-terminus for cellular CEP55 localization as in U2OS bone osteosarcoma cells the C-terminal amino acids 355–464 are required for CEP55 localization to the midbody and the centrosomes(13). However, as shown in Fig. 9A, the $CEP55^{59428}$ mutant is still bound to the centrosome and midbody.

In order to analyze the role of CEP55 MT-binding on the CIN rate, chromosomal alignment and micronuclei formation were compared between CEP55 sh1 cells and cells re-expressing $CEP55^{WT}$ or $CEP55^{59428}$. The results of these experiments revealed that re-expression of $CEP55^{59428}$ did not rescue

the reducing effect of CEP55 depletion on CIN (Fig. 9B, C). Thus, binding of CEP55 to MTs is required for its promoting effect on CIN.

Impact of CEP55 on MT-dynamics in vitro

Our cellular data show that CEP55 controls MT-dynamics but do not indicate whether CEP55 directly controls this process. To assess this, the effect of bacterial expressed CEP55 on MT-polymerization was analyzed *in vitro* by a turbidity assay. As negative controls, the $CEP55^{59428}$ and $CEP55^{127–361}$ mutants were employed. Thereby, we found that CEP55 increased the rate of MT-polymerization 4-fold while the mutants did not affect MT-polymerization (Fig. 10A-C).

Since increased MT-polymerization can result from attenuation of MT-depolymerization (catastrophe) and in cells CEP55 promotes MT-stabilization, we next assessed the impact of CEP55 on MT-stability. For this, Rhodamine labeled MTs were depolymerized in presence of 4 mM $CaCl_2$ at 4°C in absence and presence of CEP55. This experiment revealed that CEP55 protected MTs from cold-induced depolymerization (Fig. 10D).

From these results, we conclude that CEP55 directly promotes MT-polymerization, most likely by attenuating catastrophe. These data are in line with our results obtained by cell culture experiments, showing that a high level of CEP55 stabilizes MTs

Discussion

CEP55 has been first described by Fabbro et al. in 2005(13) and in parallel by Martinez-Garay et al. (2006)(14). From this time to present, more than 110 studies have been published, demonstrating the oncogenic activity of CEP55, which in normal cells is mainly expressed in thymus and in testis(13, 14). Also, many efforts have been undertaken to analyze the mechanism of how CEP55 drives tumorigenesis. The main findings are that CEP55 interacts with the p85 regulatory subunit of PI3KCA and thereby stimulates the PI3K-Akt pathway and cellular proliferation(15, 17, 22, 23). Furthermore, CEP55-mediated recruitment of TSG101 and Alix to the midbody is a crucial step for cytokinesis of many cancer cell types(13, 16). However, in normal non-neuronal cells CEP55 is not essential for cellular division, underlying its tumor-specific role(24). In addition, CEP55 is essentially involved in the control of CIN and aneuploidy. CEP55 has been identified in the proteome of the mitotic spindle(25), the protein belongs to the CIN70 score(5) and MEFs derived from CEP55 overexpressing mice show an increased CIN rate(15).

In this study we analyzed these oncogenic activities of CEP55 in OvCa cells. Interestingly, our data show that CEP55 did not affect Akt-PI3K signaling, which is constitutively activated in SKOV-3 and OVCAR-8 cells (Figure 1A). This result is in contrast to studies conducted with hepatocellular carcinoma, esophageal squamous cell carcinoma, lung cancer and MEFs, where a high CEP55 level increased Akt phosphorylation (15, 17, 22, 23). One possible explanation for this cell-typical CEP55-mediated PI3K-Akt regulation is its cellular localization. Chen et al. (22) demonstrated that in lung cancer cells CEP55 is diffusely located into the cytoplasm and in response to VEGFA stimulation translocates to the plasma

membrane, enabling the protein to interact with PI3KCA. This finding was confirmed by other studies in which the cells were stimulated with serum(17) or remained unstimulated(15, 23). Thus, in cells with a high cytosolic CEP55 concentration the protein constitutively, or in response to cellular stimulation, enhances activation of the PI3K-Akt pathway. In OvCa cells, however, CEP55 was mainly located to spindle MTs, midbody and the centrosome (Figure 9A and unpublished results), while in the cytosol only low CEP55 concentrations were detectable. Since high cytosolic CEP55 concentrations are required to activate PI3K, the low cytosolic CEP55 concentration in OvCa cells may explain why in this cell type CEP55 is not involved in the regulation of PI3K-Akt signaling.

On the other hand, we confirmed that a high level of CEP55 significantly increased the speed of midbody separation in an Alix-dependent manner, and increased the CIN rate(10). Since in contrast to the role of CEP55 in midbody separation, its function in CIN has not been elucidated yet, the focus of this study was to address this issue.

Due to the finding that CIN can be caused by dysregulation of spindle MT-dynamics(3, 6) and CEP55 has been shown to bind to MTs *in vitro*(12), we first analyzed potential spindle MT-errors in CEP55 depleted cells. Thereby, we found that down-regulation of CEP55 expression decreased spindle MT-stability and increased the speed of spindle MT-dynamics. Moreover, cell-free *in vitro* analysis revealed that recombinant CEP55 strongly increased MT-polymerization, most likely by attenuating MT-depolymerization, thus increasing MT-stability. From these data, we conclude that CEP55 over-stabilizes spindle MTs and thereby reduces its motility. The finding of Sinha et al., showing that CEP55 overexpression in MEFs increased stability of spindle MTs(15), supports this conclusion.

To validate that CEP55 controls CIN by modulating spindle MT-dynamics, we identified the yet unknown CEP55 MT-binding sites inside N-terminal (aa 1-58) as well as in C-terminal (aa 429-464) peptides. The basic unstructured N-terminus of CEP55 exhibits typical features of an MT-binding peptide(20), while the C-terminal peptide does not. However, a mutant with deleted N-terminus showed reduced but not deficient binding to MTs, showing the involvement of the C-terminus for MT binding. Since MT-binding domains can be very diverse, *cryogenic electron microscopy-based data are necessary to finally reveal the nature of the MT-CEP55 interaction(20).*

The identification of the MT-binding peptides enabled us to finally validate the requirement of CEP55-MT binding for its promoting effect on CIN. For this purpose, a mutant with deleted MT-binding peptides ($CEP55^{59-428}$) was re-expressed in OvCa shRNA cells to show whether this manipulation restore the increased CIN rate of control cells. Analysis of chromosome alignment and micronuclei formation revealed that this was not the case, although re-expression of $CEP55^{WT}$ fully rescued reduced CIN of shRNA cells. Thus, CEP55 indeed controls CIN by its MT-modulating activity. This conclusion is supported by experiments where expression of the MT-depolymerizing kinesin KIF2B reversed the increased CIN rate in CEP55 overexpressing MEFs(15). In conclusion, our data show that in OvCa metaphase cells a high level of CEP55 stabilizes spindle MTs and thereby reduces MT-dynamics. Due to this impaired spindle

MT-dynamics in cells with high CEP55 levels chromosomes are not properly aligned in metaphase resulting in chromosome mis-segregation, and thus in CIN.

Together, we demonstrate that in OvCa cells CEP55 does not affect constitutively activated PI3K-Akt signaling but controls midbody separation and CIN in a dose-dependent manner. Moreover, for the first time we show that CEP55 increases CIN by its MT-binding activity, most likely by over-stabilizing spindle MTs. Thus, selective interfering with CEP55-MT binding may block its CIN-promoting effect.

Materials And Methods

Cell culture and stable lentiviral knock-down of CEP55

SKOV-3 cells were cultivated in McCoy's 5A medium (26600-023, Gibco) containing 10% (v/v) FCS, 2 mM Glutamine and Pen/Strep (100 units/ml penicillin, 100 µg/ml streptomycin). OVCAR-8 cells were cultivated in RPMI medium (72400-21, Gibco) containing 10% (v/v) FCS and Pen/Strep (100 units/ml penicillin, 100 µg/ml streptomycin). In SKOV-3 and OVCAR-8 ovarian carcinoma cells a stable knock-down of CEP55 was performed as described before(26). Vectors from the mission shRNA system from Sigma-Aldrich were used for lentiviral transduction. Five different CEP55 shRNA constructs in the TRC2-pLKO.1 lentiviral vectors were tested. After selection with puromycin (3 µg/ml) the two cell lines with the strongest knockdown were selected (CEP55 sh1 and sh2). The targeted sequence of sh1 (TRCN000006197) is CCGGGCAGGCATGTACTTTAGACTTCTCGAGAAGTCTAAAGTACATGCCTGCTTTTTG. Sh2 (TRCN0000061975) targets the sequence CCGGGCAGCATCAATTGCTTGTAATCTCGAGATTACAAGCAATTGATGCTGCTTTTTG. Cells stably expressing scrambled shRNA were used as control.

Stable lentiviral re-expression of $CEP55^{WT}$, $CEP55^{Y187A}$ and $CEP55^{59-428}$

To generate the ALIX or MT-binding mutants $CEP55^{Y187A}$ or $CEP55^{59-428}$ quick change mutagenesis was performed.

For stable re-expression of $CEP55^{WT}$, $CEP55^{Y187A}$ and $CEP55^{59-428}$ the genes were cloned into the LeGo-iB_2 Neo+ vector (a friendly gift from Kristoffer Riecken, UKE). The empty vector was used as control. Stable lentiviral re-expression of the proteins into CEP55 sh1 cells was performed as described (27). 72 h after the last virus-infection the cells were selected using 700 µg/ml G418. Re-expression was analyzed by Western blotting.

Western Blotting

Western blot analysis was performed by a standard procedure using nitrocellulose membranes. For CEP55 (anti-rabbit, #81693, cell signalling), Akt (anti-rabbit, #9272, cell signalling), phosphoAkt (anti-rabbit, #4058, cell signalling) and GFP (anti-mouse, 11814460001, Roche) antibodies the membranes

were blocked for 30 min RT with 5% milk powder in Tris-buffered saline and Tween20 (TBS-T). For β-Tubulin (anti-mouse, T4026, Sigma) 2.5% BSA/TBS-T was used for blocking. HSC70 (anti-mouse, sc-7298, santa cruz) worked with both blocking methods. The secondary antibodies against mouse (ab205719, abcam) or rabbit (ab205718, abcam) were diluted in TBS-T and incubated for 1 hour at RT. For signal production and detection chemiluminescence reagent (Amersham ECL Prime Western Blotting Detection Reagent, GE Healthcare Bio-Sciences) and the Intas ECL CHEMOCAM imager were used. Band intensities were quantified by Fiji (NIH National Institutes of Health) and normalized to HSC70.

Real time PCR

To analyze the mRNA expression level of CEP55 a standard quantitative RT-PCR (qPCR) was performed. From cell pellets the whole mRNA was extracted and cDNA generated using oligo dT primers. Samples were analyzed in triplicates with the QuantStudio™ 3 System (AppliedBiosystems). CEP55 mRNA expression was evaluated using the following primers: CEP55 FW (GTCTGCTGCAACCTCACGAA) and CEP55 RV (AGCAGTTTGGAGCCACAGTC). GAPDH was used as internal control (GAPDH FW: AGTCCCTGCCACACTCAG, GAPDH RV: TACTTTATTGATGGTACATGACAAGG). The relative CEP55 expression was calculated using the ΔΔCt method and normalized to scr + L control cells.

Immunofluorescence staining

2 x 10^4 cells were seeded into chamber slides (Ibidi). For β -tubulin staining, cells were fixed with 4% Paraformaldehyde/DMEM + 10% FCS for 10 min at 37 °C, permeabilized 3 x with 0.1% Triton-X-100/PBS for each 5 min at RT. The β-tubulin antibody (T4026, Sigma) was diluted 1:200 in 4% FCS/PBS and incubated over-night at 4 °C. For detyrosinated α-tubulin (ab48389, abcam) or CEP55 staining, cells were fixed in ice cold methanol at -20 °C. The washing steps were performed with 0.05% Triton-X-100/PBS. Cells were blocked with 1% BSA in 0.05% Triton-X-100/PBS for 1 hour. The antibody was diluted 1:200 in blocking solution and incubated for 1 hour at room temperature. For co-staining the β -tubulin antibody was used after the detyrosinated α-tubulin or CEP55 antibody. Secondary antibodies were anti-rabbit Alexa-fluor®488 (A21206, life technologies) and anti-mouse Alexa-fluor®568 (A11031, life technologies), both diluted 1:2000 in PBS and incubated for 1 hour at RT. DNA was stained by 4',6-diamidino-2-phenylindole (DAPI) in a 1:2000 dilution, 2 min RT. Images were obtained with Olympus IX83 or with Leica TCS SP8 X microscope.

Analysis of cellular MT dynamics by live cell imaging

To assess MT dynamics in living cells, cells were labelled with SiR-Tubulin (#CY-SC006, Cytoskeleton), a small molecule that specifically binds to microtubules and is well suited to assess MT-dynamics in cells(28). For live cell imaging, 0.5 x 10^4 cells were seeded into chamber slides and incubated for 48 hours. After 48 hours, the medium was changed to 0.5 µM SiR-Tubulin containing medium and the cells were incubated for four more hours. After incubation with SiR-Tubulin, the medium was changed to 50 nM Hoechst 33342 (H3570, Invitrogen) containing medium. Z-stacked images were obtained every five minutes over 15 hours using the Visitron Spinning Disk microscope (UKE Microscopy Imaging Facility),

connected to an incubation chamber with 37 °C, 5% CO_2 and humidity. IMARIS software (Oxford Instruments) was used for 3-D-reconstruction and data evaluation of microtubule speed in late metaphase.

Chromosome isolation

Chromosomes were isolated as described (29). Thereafter, chromosomes were analysed by microscopy and the number of chromosomes per nucleus was determined.

Next Generation Sequencing

DNA isolated from control and CEP55 knock-down SKOV-3 and OVCAR-8 cells underwent PCR-free, DNA nanoball, Next Generation Sequencing (BGI, Denmark). Sequencing data was processed as before (30) with minor adjustments: fastq files were processed by fastp(31), followed by alignment to the hg38 reference genome using bwa-mem2. Copy number alterations (CNA) were estimated using control-FREEC's segmentation algorithm(32). Statistical analyses and visualization were performed using R version 4.1.1 (R Foundation for Statistical Computing) and In-Silico Online version 2.3.1 (http://in-silico.online).

Structure prediction of CEP55

The secondary structure of the CEP55 protein was predicted by using different prediction programs. For evaluation of α-helix, ß-sheet and random coil probability PSIPRED, PredictProteinOpen, NetSurfP-1.1, NetSurfP-2.0 and RaptorX SS8 were used, and for prediction of coiled-coil structures DeepCoil1, DeepCoil2, Marcoil and Ncoil (33-41). The 3D structure of the CEP55 protein was predicted from its amino acid sequence using the DeepMind program AlphaFold(21).

Recombinant expression of His-GFP-CEP55 and CEP55 mutants

CEP55 gene was codon optimized for expression in *E. coli* strains and cloned into the psf421 vector to get His-GFP fusion proteins. Mutations were inserted by SLIC cloning.

Proteins were expressed in Rosetta 2(DE3)pLysS *E. coli*. The bacteria were incubated in Terrific Broth (TB) medium, shaked at 37°C until OD600 of one and protein expression was induced with 0.1 mM IPTG. After incubation over-night at 16 °C, bacteria were harvested (3700 x g, 10 min, 4 °C) and washed with PBS. For cell lysis, the pellet was resuspended in lysis-buffer (20 mM HEPES pH 7.5, 400 mM NaCl, 1 mM EDTA, 1 mM DTT, 0.5 mM benzamidine). After disruption with the cell homogenizer (Constant Systems Ltd CF1) at 1.8 kbar, 1 mM PMSF and 0.1% Triton-X-100 were added. Prior to centrifugation (48000 x g, 30 min, 4 °C) 25 mM Imidazole was added and incubated for 5 min. The protein lysate was incubated with equilibrated Ni-NTA Agarose (R901, Invitrogen) for 1 h at 4 °C. Beads with lysate were applied to a column and washed with 20 mM HEPES pH 7.5, 400 mM NaCl, 0.1% Triton-X-100 and 25 mM Imidazole. Followed by an incubation with 10 mM ATP and 20 mM $MgCl_2$ in 20 mM HEPES pH 7.5, 400 mM NaCl and 25 mM Imidazole for 25 min. Beads were washed with increasing Imidazole concentrations (35, 50, 62.5 and 75

mM Imidazole). Elution was performed twice with 20 mM HEPES pH 7.5, 400 mM NaCl and 130, respectively, 150 mM Imidazole and 1 mM PMSF. Proteins were dialysed overnight at 4 °C to 20 mM HEPES pH 7.5, 250 mM NaCl and 1 mM DTT. The protein concentration of elution-fractions was quantified with a BSA standard by SDS-PAGE stained with Roti Blue quick (4829.1, Roth). Proteins were frozen in liquid nitrogen and stored at -80 °C.

MT-Binding

To analyse binding of MTs to recombinant expressed GFP, GFP-CEP55 and GFP-CEP55 mutants, the proteins were bound to equilibrated GFP-Trap® Magnetic Agarose Beads GFP (ChromoTek). 355 nM of protein were incubated for 1 h at 4 °C with 15 µl beads solution in 20 mM HEPES pH 7.5, 250 mM NaCl, 1 mM DTT. After incubation, beads were washed twice with buffer to remove unbound protein. To assess binding of MTs to CEP55-coupled agarose beads, tubulin prepared from porcine brain (for protocol, see https://hymanlab.org/hyman_lab/) was applied and polymerized as follows: 0.15 µM taxol were added to the tubulin solution (545 nM in 80 mM PIPES pH 6.8, 2 mM $MgCl_2$ and 1 mM EGTA, 1 mM GTP) and incubated for 5 min at 37 °C. The taxol concentration was increased every 5 min to 1, 5 and finally to 20 µM. After polymerisation, MTs were cooled, pH was adapted to 7.5, and MTs were incubated with the immobilised GFP proteins for 1 h at 4°C. After incubation, the beads were washed 6-times with 500 µl of 50 mM HEPES/pH 7.5, 1 mM $MgCl_2$, 1 mM EGTA, 2.5 mM KCl and 0.5 mM DTT, and binding of MTs to CEP55 was analysed by Western blotting, employing an antibody against b tubulin.

MT-pulldown

To assess binding of CEP55 to MTs a classical pulldown assay was performed, adapted from the Cytoskeleton Microtubule Binding Protein Spin-down Assay Kit (BK029). Here, MT-bound CEP55 co-precipitates with MTs.

MT-polymerisation was performed as described above in general tubulin buffer and MT solution was diluted to an end concentration of 400 ng/µl, CEP55 proteins were applied in a concentration of 200 nM. The proteins were carefully placed on top of a taxol supplemented glycerol cushion (general tubulin buffer with 60% glycerol and 20 µM taxol), and after centrifugation at 100,000 g and 23 °C for 40 min the uppermost 50 µl of the supernatant were transferred into sample buffer. The remaining cushion buffer was discarded and the pellet resuspended in sample buffer. Supernatant and corresponding pellets were analysed by Western blotting employing a GFP antibody. For evaluation, the percentage of protein bound to tubulin was determined.

MT-polymerisation

To analyse MTs by fluorescence microscopy, rhodamine labelled tubulin (#TL590M, Cytoskeleton) was prepared as described (27). 250 nM tubulin and 250 nM CEP55 proteins were mixed and incubated at 37 °C for 30 min. After incubation, 10 µl of the tubulin-protein solution were pipetted on a chamber slide,

again incubated for 10 min and coated with 30 µl Fluoromount G (SouthernBiotech). The sample was imaged by confocal microscopy (TCS SP8 (Leica)).

Analysis of MT-polymerisation was performed by a turbidity assay as described (27). For this experiment, 237 nM CEP55 proteins (diluted in general tubulin buffer) and 3 µM self-prepared tubulin (see above) were mixed with 1 mM GTP, general tubulin buffer (80 mM PIPES pH 6.8, 2 mM $MgCl_2$ and 1 mM EGTA) and 10% DMSO. Polymerisation was measured in a Tecan Infinite 200 reader as absorption at 340 nm at 37 °C.

Cold-induced MT-depolymerisation

To analyze the effect of CEP55 on MT stability, the cold-induced MT-depolymerization assay was performed. Rhodamine labeled, taxol stabilized MTs were prepared as described (27). 250 nM of CEP55 proteins and 250 nM rhodamine labelled tubulin were mixes and incubated for 10 min at room temperature. For cold-induced depolymerization, the CEP55-tubulin mixture was incubated at 4 °C for 10 min in presence of 4 mM $CaCl_2$. 10 µl of the tubulin-protein solution were applied to a chamber slide, coated with 30 µl Fluoromount G (SouthernBiotech) and imaged with the Olympus IX83 microscope.

Declarations

Ethics approval and consent to participate

Not applicable

Consent for publication

Not applicable

Availability of data and material

The datasets used and analysed during the current study are available from the corresponding author on reasonable request.

Competing interests

The authors declare that they have no competing interests.

Funding

This study was supported by a grant from the Wilhelm Sander-Stiftung (2017.103.1) to SW.

with chromosome preparation and Christine Blechner for excellent technical support.

Authors’ contribution

Conceptualization: SW. Formal analysis: SM, PS, TP, SJ. Funding acquisition: SW. Investigation: SM, PS, TP, and SJ. Methology: SM, PS, TP, SJ. Project administration: SW, SM. Resources: SW. Supervision: SW. Validation: SM, PS, TP, SJ. Visualization: SM, PS. Writing – original draft: SW. Writing – reviewing & editing: SW, SM, PS, TP, SJ. The authors read and approved the final manuscript.

Acknowledgement

We acknowledge the UKE Microscopic Imaging Facility (UMIF). We thank Kira Schamoni and Saskia Grüb for helping to analyze MT-CEP55 interactions and for helping with chromosome preparation. Also we thank Yannes Popp for helping to establish microtubule life cell imaging and Christine Blechner for excellent technical support. This study was supported by a grant from the Wilhelm Sander-Stiftung (2017.103.1) to S.W.

Authors' information

Dr. Stefanie Muhs (PhD): PostDoc at Department of Biochemistry and Signal Transduction. This work includes the main part of her PhD thesis performed at the Department of Biochemistry and Signal Transduction at the University Medical Center Hamburg-Eppendorf. Paula Schaefer (PhD student): Department of Biochemistry and Signal Transduction, University Medical Center Hamburg-Eppendorf. Themis Paraschiakos: (PhD student): Department of Biochemistry and Signal Transduction, University Medical Center Hamburg-Eppendorf. Dr. Simon Joosse (PhD): Group leader at the department of Tumor Biology at University Medical Center Hamburg-Eppendorf. Prof. Dr. Sabine Windhorst (PhD): Professor at Department of Biochemistry and Signal Transduction, University Medical Center Hamburg-Eppendorf.

References

1. Kim S, Han Y, Kim SI, Kim HS, Kim SJ, Song YS. Tumor evolution and chemoresistance in ovarian cancer. NPJ Precis Oncol. 2018;2:20.
2. Tamura N, Shaikh N, Muliaditan D, Soliman TN, McGuinness JR, Maniati E, et al. Specific Mechanisms of Chromosomal Instability Indicate Therapeutic Sensitivities in High-Grade Serous Ovarian Carcinoma. Cancer Res. 2020;80(22):4946-59.
3. Potapova TA, Zhu J, Li R. Aneuploidy and chromosomal instability: a vicious cycle driving cellular evolution and cancer genome chaos. Cancer Metastasis Rev. 2013;32(3-4):377-89.
4. Sansregret L, Swanton C. The Role of Aneuploidy in Cancer Evolution. Cold Spring Harb Perspect Med. 2017;7(1).
5. Carter SL, Eklund AC, Kohane IS, Harris LN, Szallasi Z. A signature of chromosomal instability inferred from gene expression profiles predicts clinical outcome in multiple human cancers. Nat Genet. 2006;38(9):1043-8.
6. Bakhoum SF, Thompson SL, Manning AL, Compton DA. Genome stability is ensured by temporal control of kinetochore-microtubule dynamics. Nat Cell Biol. 2009;11(1):27-35.

7. Pino MS, Chung DC. The chromosomal instability pathway in colon cancer. Gastroenterology. 2010;138(6):2059-72.
8. Huang Y, Jiang L, Yi Q, Lv L, Wang Z, Zhao X, et al. Lagging chromosomes entrapped in micronuclei are not 'lost' by cells. Cell Res. 2012;22(5):932-5.
9. Zhang W, Niu C, He W, Hou T, Sun X, Xu L, et al. Upregulation of centrosomal protein 55 is associated with unfavorable prognosis and tumor invasion in epithelial ovarian carcinoma. Tumour Biol. 2016;37(5):6239-54.
10. Jeffery J, Sinha D, Srihari S, Kalimutho M, Khanna KK. Beyond cytokinesis: the emerging roles of CEP55 in tumorigenesis. Oncogene. 2016;35(6):683-90.
11. Schiewek J, Schumacher U, Lange T, Joosse SA, Wikman H, Pantel K, et al. Clinical relevance of cytoskeleton associated proteins for ovarian cancer. Journal of cancer research and clinical oncology. 2018;144(11):2195-205.
12. Zhao WM, Seki A, Fang G. Cep55, a microtubule-bundling protein, associates with centralspindlin to control the midbody integrity and cell abscission during cytokinesis. Mol Biol Cell. 2006;17(9):3881-96.
13. Fabbro M, Zhou BB, Takahashi M, Sarcevic B, Lal P, Graham ME, et al. Cdk1/Erk2- and Plk1-dependent phosphorylation of a centrosome protein, Cep55, is required for its recruitment to midbody and cytokinesis. Dev Cell. 2005;9(4):477-88.
14. Martinez-Garay I, Rustom A, Gerdes HH, Kutsche K. The novel centrosomal associated protein CEP55 is present in the spindle midzone and the midbody. Genomics. 2006;87(2):243-53.
15. Sinha D, Nag P, Nanayakkara D, Duijf PHG, Burgess A, Raninga P, et al. Cep55 overexpression promotes genomic instability and tumorigenesis in mice. Commun Biol. 2020;3(1):593.
16. Lee HH, Elia N, Ghirlando R, Lippincott-Schwartz J, Hurley JH. Midbody targeting of the ESCRT machinery by a noncanonical coiled coil in CEP55. Science. 2008;322(5901):576-80.
17. Chen CH, Lu PJ, Chen YC, Fu SL, Wu KJ, Tsou AP, et al. FLJ10540-elicited cell transformation is through the activation of PI3-kinase/AKT pathway. Oncogene. 2007;26(29):4272-83.
18. Bakhoum SF, Genovese G, Compton DA. Deviant kinetochore microtubule dynamics underlie chromosomal instability. Curr Biol. 2009;19(22):1937-42.
19. Janke C, Magiera MM. The tubulin code and its role in controlling microtubule properties and functions. Nat Rev Mol Cell Biol. 2020;21(6):307-26.
20. Manka SW, Moores CA. Microtubule structure by cryo-EM: snapshots of dynamic instability. Essays Biochem. 2018;62(6):737-51.
21. Jumper J, Evans R, Pritzel A, Green T, Figurnov M, Ronneberger O, et al. Highly accurate protein structure prediction with AlphaFold. Nature. 2021;596(7873):583-9.
22. Chen CH, Lai JM, Chou TY, Chen CY, Su LJ, Lee YC, et al. VEGFA upregulates FLJ10540 and modulates migration and invasion of lung cancer via PI3K/AKT pathway. PLoS One. 2009;4(4):e5052.

23. Jia Y, Xiao Z, Gongsun X, Xin Z, Shang B, Chen G, et al. CEP55 promotes the proliferation, migration and invasion of esophageal squamous cell carcinoma via the PI3K/Akt pathway. Onco Targets Ther. 2018;11:4221-32.
24. Tedeschi A, Almagro J, Renshaw MJ, Messal HA, Behrens A, Petronczki M. Cep55 promotes cytokinesis of neural progenitors but is dispensable for most mammalian cell divisions. Nat Commun. 2020;11(1):1746.
25. Sauer G, Korner R, Hanisch A, Ries A, Nigg EA, Sillje HH. Proteome analysis of the human mitotic spindle. Mol Cell Proteomics. 2005;4(1):35-43.
26. Windhorst S, Fliegert R, Blechner C, Mollmann K, Hosseini Z, Gunther T, et al. Inositol 1,4,5-trisphosphate 3-kinase-A is a new cell motility-promoting protein that increases the metastatic potential of tumor cells by two functional activities. J Biol Chem. 2010;285(8):5541-54.
27. Heinz LS, Muhs S, Schiewek J, Grub S, Nalaskowski M, Lin YN, et al. Strong fascin expression promotes metastasis independent of its F-actin bundling activity. Oncotarget. 2017;8(66):110077-91.
28. Lukinavicius G, Reymond L, D'Este E, Masharina A, Gottfert F, Ta H, et al. Fluorogenic probes for live-cell imaging of the cytoskeleton. Nat Methods. 2014;11(7):731-3.
29. Grueb SS, Muhs S, Popp Y, Schmitt S, Geyer M, Lin YN, et al. The formin Drosophila homologue of Diaphanous2 (Diaph2) controls microtubule dynamics in colorectal cancer cells independent of its FH2-domain. Sci Rep. 2019;9(1):5352.
30. Riebensahm C, Joosse SA, Mohme M, Hanssen A, Matschke J, Goy Y, et al. Clonality of circulating tumor cells in breast cancer brain metastasis patients. Breast Cancer Res. 2019;21(1):101.
31. Chen S, Zhou Y, Chen Y, Gu J. fastp: an ultra-fast all-in-one FASTQ preprocessor. Bioinformatics. 2018;34(17):i884-i90.
32. Boeva V, Popova T, Bleakley K, Chiche P, Cappo J, Schleiermacher G, et al. Control-FREEC: a tool for assessing copy number and allelic content using next-generation sequencing data. Bioinformatics. 2012;28(3):423-5.
33. Buchan DWA, Jones DT. The PSIPRED Protein Analysis Workbench: 20 years on. Nucleic Acids Res. 2019;47(W1):W402-W7.
34. Delorenzi M, Speed T. An HMM model for coiled-coil domains and a comparison with PSSM-based predictions. Bioinformatics. 2002;18(4):617-25.
35. Gabler F, Nam SZ, Till S, Mirdita M, Steinegger M, Soding J, et al. Protein Sequence Analysis Using the MPI Bioinformatics Toolkit. Curr Protoc Bioinformatics. 2020;72(1):e108.
36. Jones DT. Protein secondary structure prediction based on position-specific scoring matrices. J Mol Biol. 1999;292(2):195-202.
37. Klausen MS, Jespersen MC, Nielsen H, Jensen KK, Jurtz VI, Sonderby CK, et al. NetSurfP-2.0: Improved prediction of protein structural features by integrated deep learning. Proteins. 2019;87(6):520-7.

38. Ludwiczak J, Winski A, Szczepaniak K, Alva V, Dunin-Horkawicz S. DeepCoil-a fast and accurate prediction of coiled-coil domains in protein sequences. Bioinformatics. 2019;35(16):2790-5.
39. Petersen B, Petersen TN, Andersen P, Nielsen M, Lundegaard C. A generic method for assignment of reliability scores applied to solvent accessibility predictions. BMC Struct Biol. 2009;9:51.
40. Yachdav G, Kloppmann E, Kajan L, Hecht M, Goldberg T, Hamp T, et al. PredictProtein--an open resource for online prediction of protein structural and functional features. Nucleic Acids Res. 2014;42(Web Server issue):W337-43.
41. Zimmermann L, Stephens A, Nam SZ, Rau D, Kubler J, Lozajic M, et al. A Completely Reimplemented MPI Bioinformatics Toolkit with a New HHpred Server at its Core. J Mol Biol. 2018;430(15):2237-43.

Figures

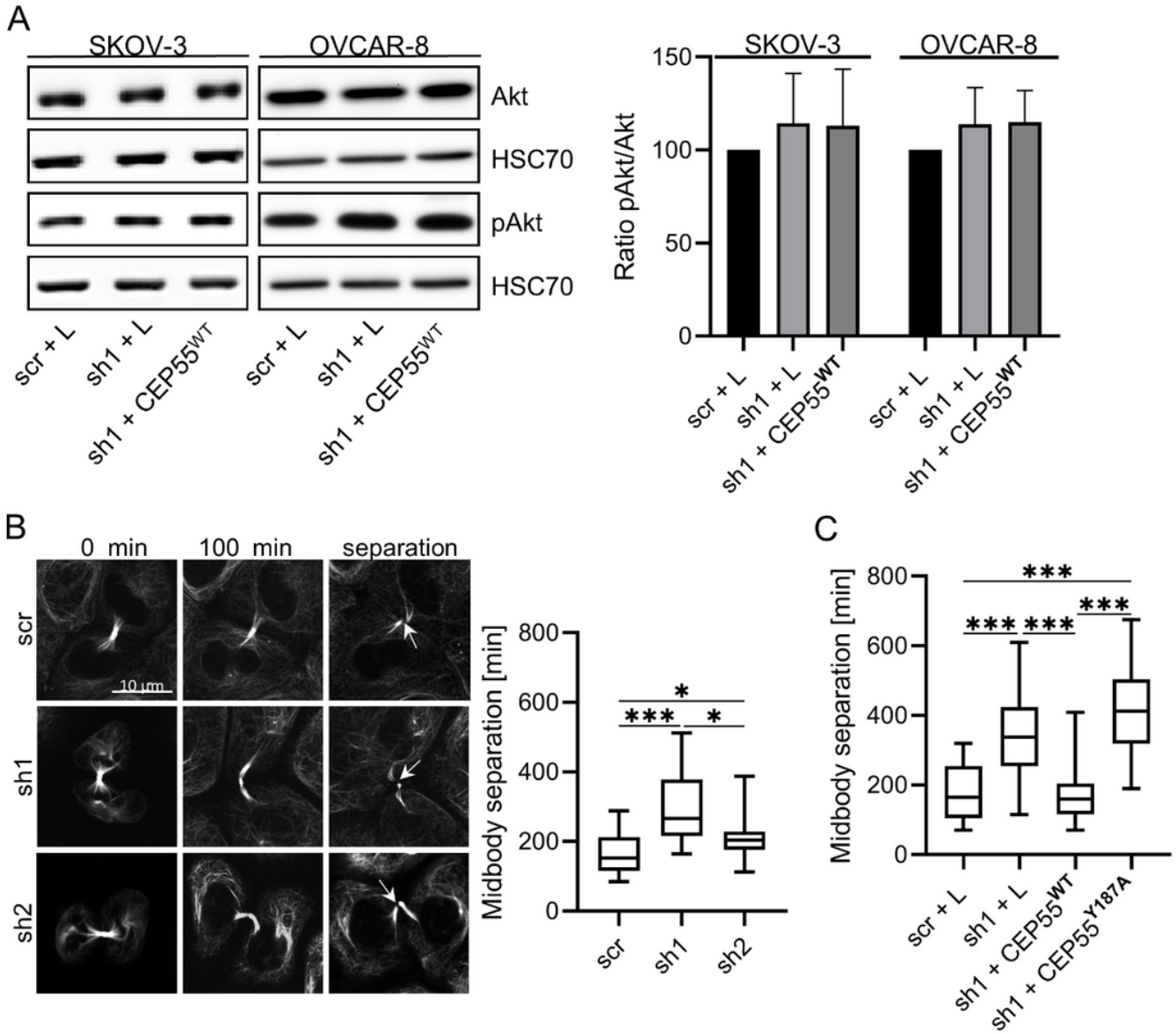

Figure 1

CEP55 does not regulate the level of pAkt but midbody separation. (A) Akt phosphorylation was assessed by Western blotting, using antibodies against pAkt and panAkt. Right panel shows signal intensities of pAkt levels normalized to panAkt levels. Shown are mean + SD from three independent experiments. **(B)** Cells were loaded with SiR tubulin and Z-stacks were imaged from the beginning of midbody formation until midbody separation every 4 min by confocal fluorescence microscopy. From Z-stacks 3-D reconstructions were performed and spatial and temporally speed of MTs was calculated using the IMARIS software. **(D)** Mean values of the time (min) necessary for midbody separation for 15 cells ± SD are shown. Significance was determined using t-test. *$p<0.05$, ***$p<0.0001$.

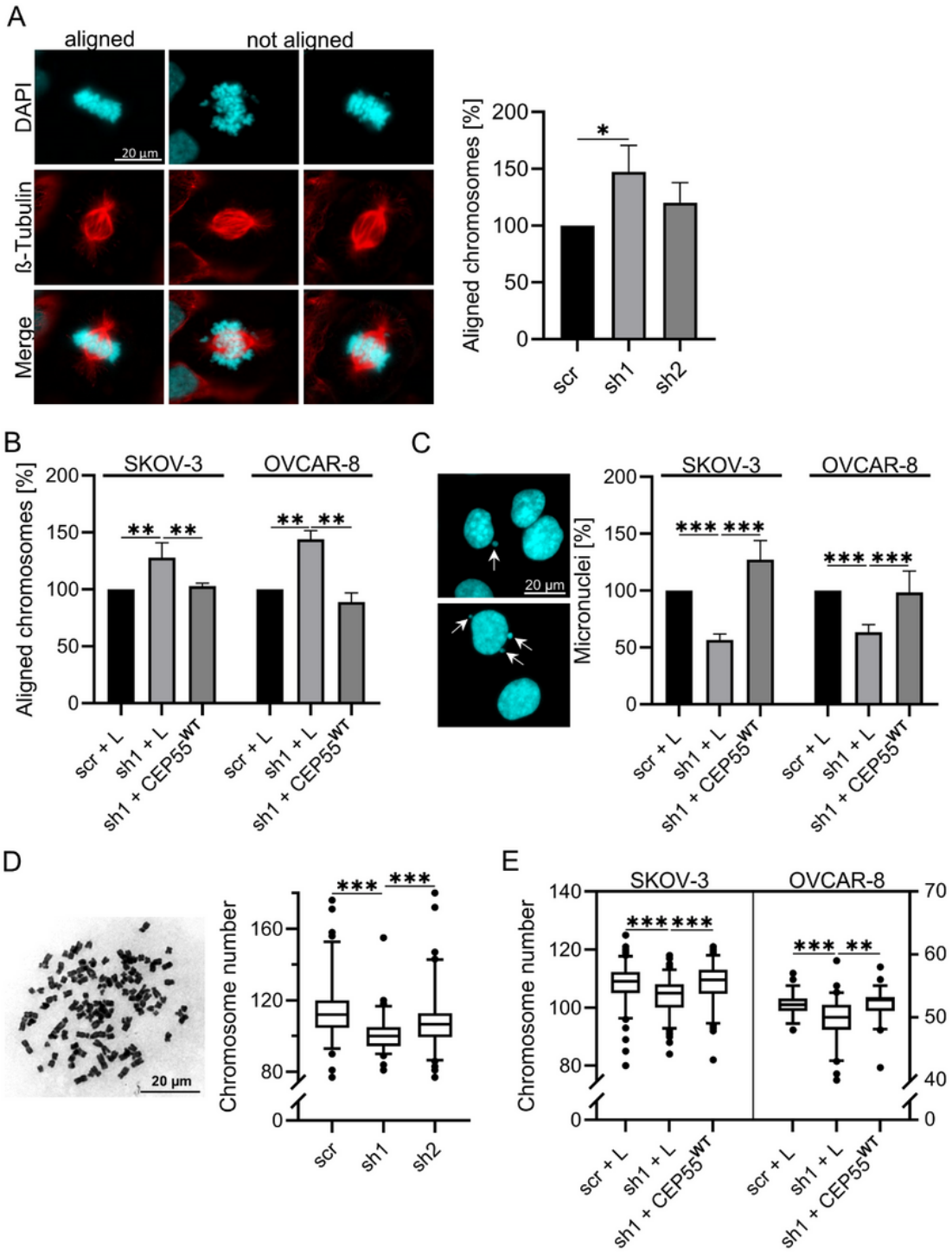

Figure 2

CEP55 depletion decreases the CIN rate in OvCa cells. (A) Metaphase cells were stained with Alexa-fluor568 coupled antibodies against b-tubulin and DAPI. **(B)** The cells were grouped in cell populations with aligned or not aligned chromosomes and counted. The number of scr control cells with aligned chromosomes was set to 100%. **(C)** Fixed interphase cells were stained with DAPI, the number of cells having micronuclei (indicated by arrows) were counted and the percentage of cells with micronuclei was

calculated. **(D)** Chromosomes from metaphase control and CEP55 shRNA cells were prepared and chromosome number per cell was determined from 80 nuclei, obtained by three different preparations. Finally, chromosome heterogeneity was calculated by the F-test. *p<0.05, **p<0.001, ***p<0.0001.

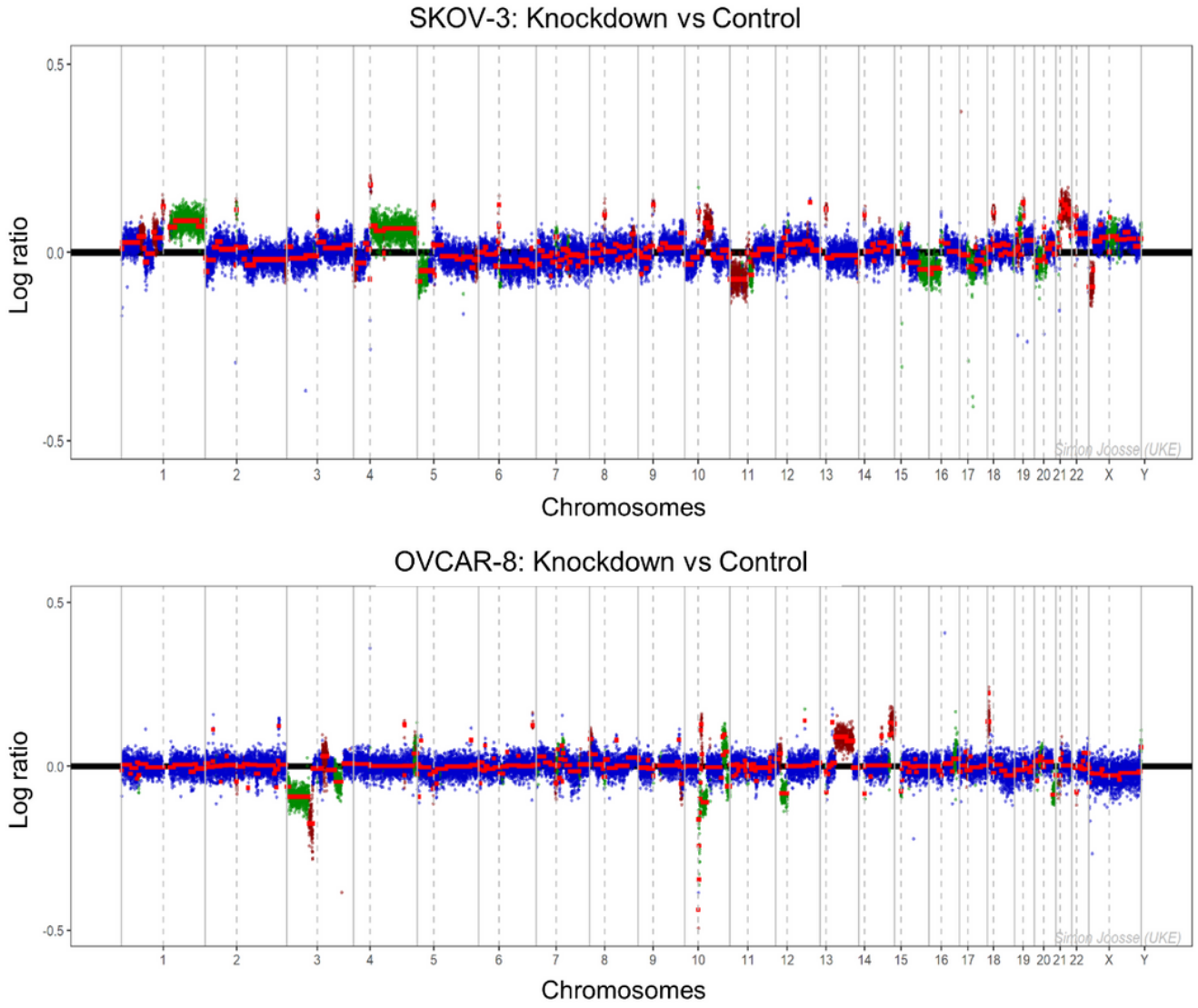

Figure 3

Knock-down of CEP55 decreases genomic heterogeneity in OvCa cells. Bold black lines represents the median copy number of chromosomes in control cells. One dot symbolizes 500 kb of copy number measurement. Median number of chromosome regions of knock-down cells were subtracted from those of control cells. Blue dots: unchanged within 2*var(MedianRatio); dark red: regions further away from

baseline in knock-down as compared to control. Green: regions closer to baseline in knockdown as compared to control.

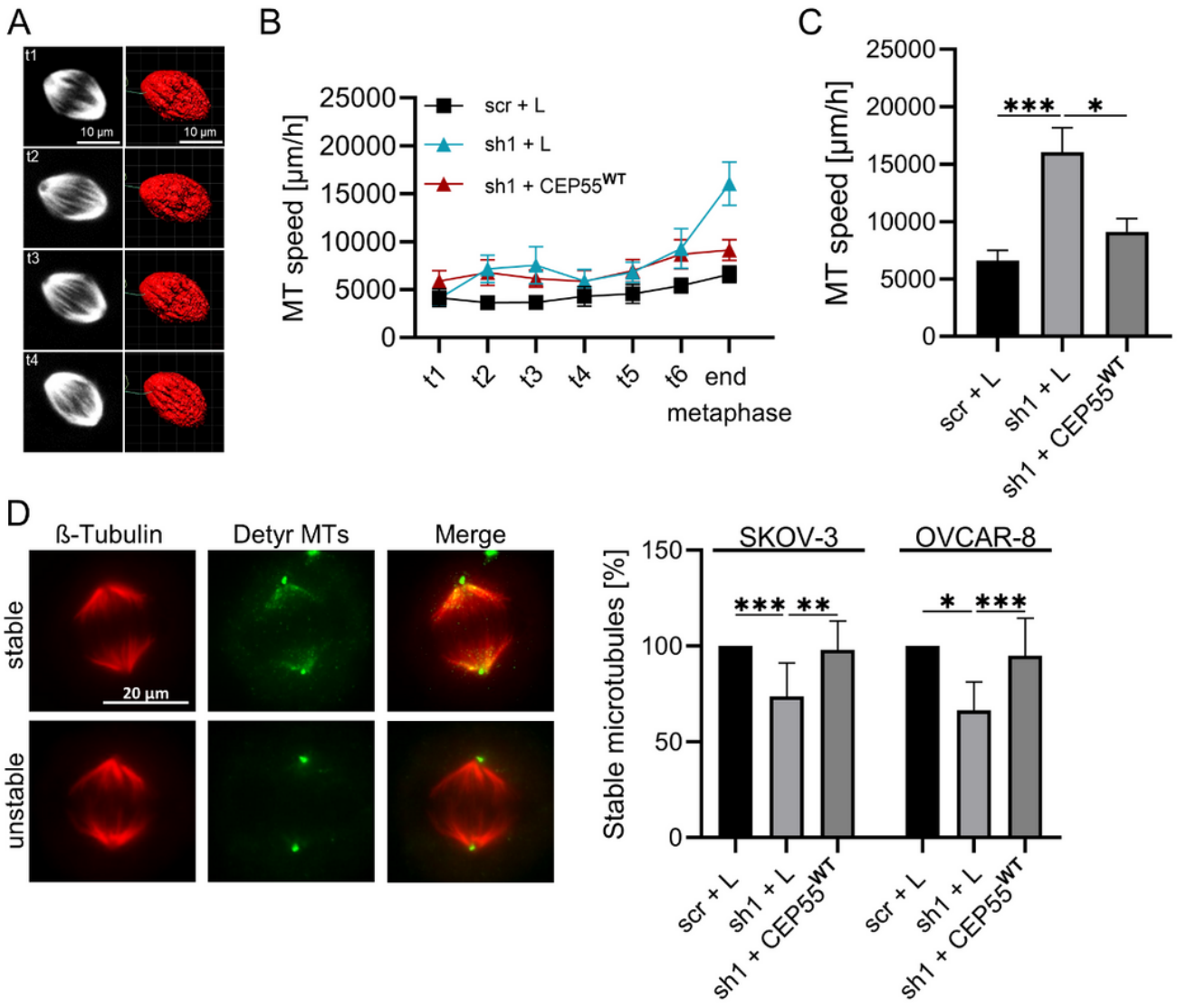

Figure 4

Down-regulation of CEP55 in OvCa cells increases spindle MT-dynamics and decreases stability spindle MTs. (A) Cells were loaded with SiR tubulin and Z-stacks were imaged from early to late metaphase every 5 min using confocal fluorescence microscopy. From Z-stacks 3-D reconstructions were performed and spatial and temporally speed (µm/h) of MTs was calculated using the Imaris software. **(B)** MT mean speed from early until late metaphase is shown. **(C)** Mean MT speed from early/late metaphase cells. Shown are mean values of 12 cells + SD. **(D)** Fixed metaphase cells were stained with Alex-Fluor568

coupled antibody against MTs (red) and with Alex-Fluor488 coupled antibody against detyrosinated MTs (green). Bar: 20 µm. Metaphase cells with stable MTs only in the spindle pole (unstable MTs) or with stable MTs in the spindle pole and in the spindle (stable MTs) were counted and the percentage of cells with stable and unstable spindle MTs were calculated. Shown are mean values + SD of 30 cells of four different experiments. *p<0.05, **p<0.005, ***p<0.0001.

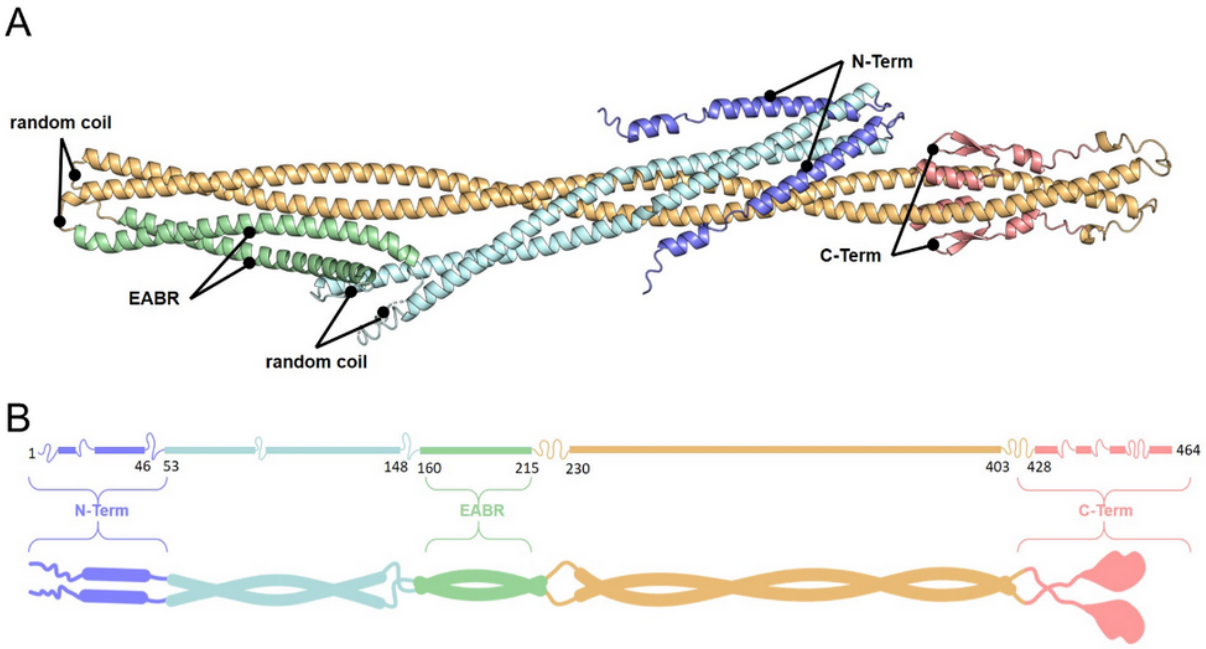

Figure 5

Prediction of the CEP55 3-D structure. (A) CEP55 is predicted by AlphaFold to be a dimer **(B)** Cartoon showing the predicted domains obtained by AlphaFold and bioinformatics (see Figure S2).

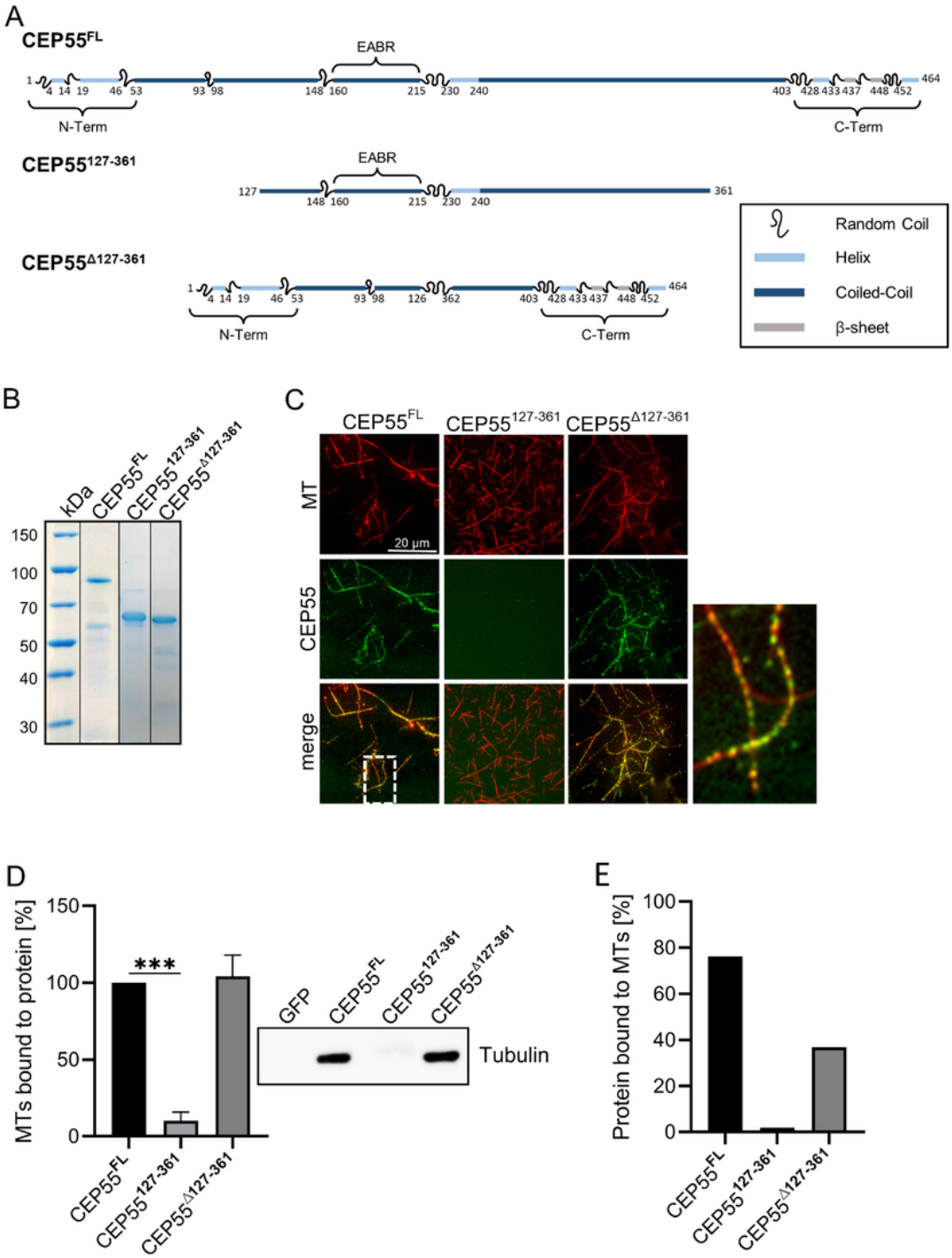

Figure 6

Amino acids 127-361 of CEP55 are not involved in MT-binding. (A) In order to identify the MT-binding domain inside the CEP55 molecule, CEP55 mutants were created as indicated in the Figure. **(B)** CEP55 wt protein ($CEP55^{FL}$) as well as mutants were expressed in *E. coli* as His-GFP fusion proteins and enriched by nickel-chelate chromatography. **(C)** $CEP55^{FL}$ or CEP55 mutants were co-incubated with Rhodamine-labeled MTs (red) and analyzed by fluorescence microscopy. **(D)** GFP, $CEP55^{FL}$ or CEP55 mutants were

coupled to GFP dynabeads and incubated with MTs. Binding of MTs to CEP55 was assessed by Western blotting. **(E)** MTs were pulled down by ultracentrifugation and the concentration of CEP55 in pellet and supernatant was analyzed by Western-botting. The percentage of CEP55 in the pellet fraction was calculated. Shown are mean values + SD of three independent experiments. *p<0.5, **p<0.005, ***p<0.0001.

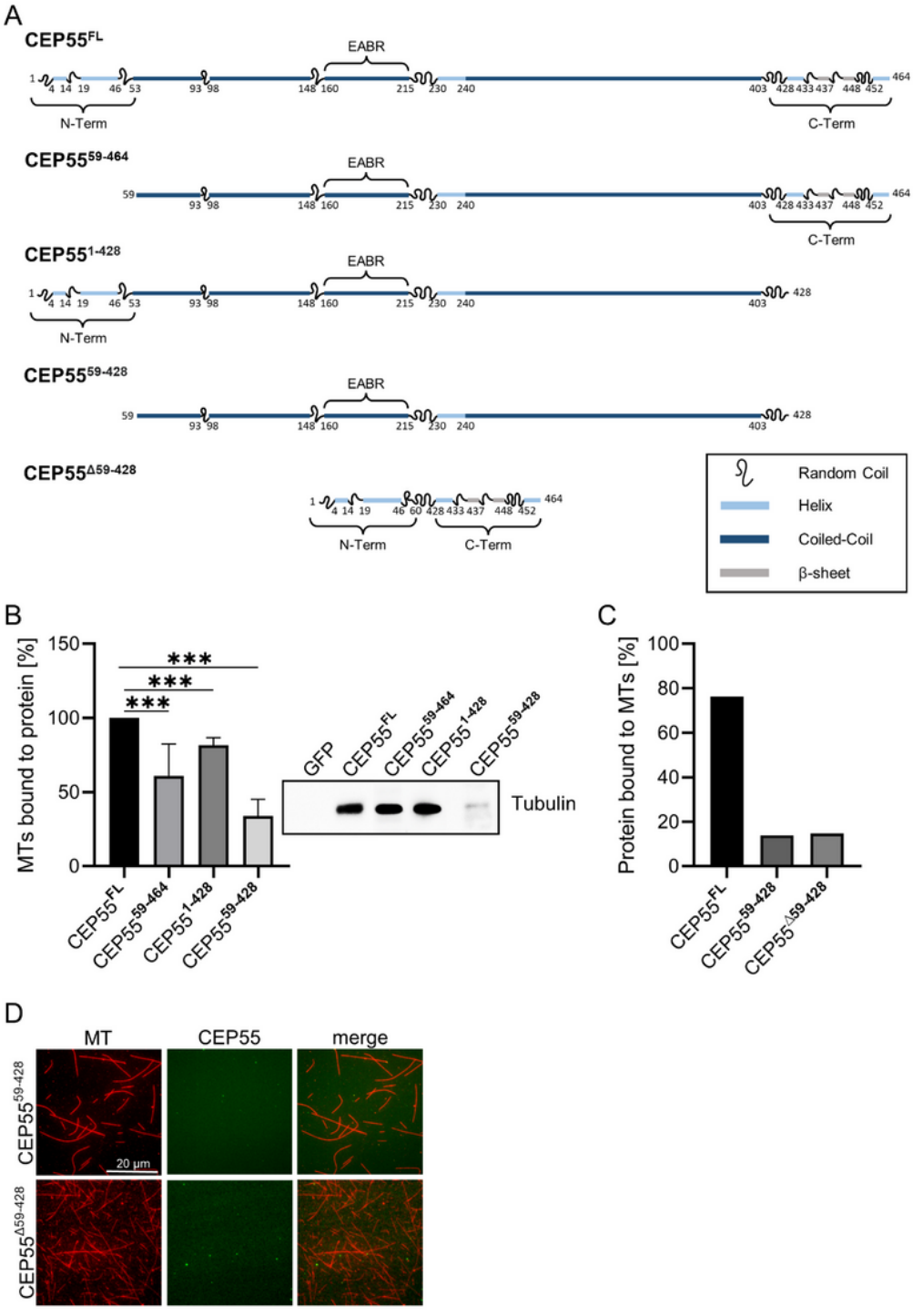

Figure 7

The CEP55 MT-binding peptides reside in the N- and the C-termini. (A) CEP55 mutants were created as indicated in the Figure**. (B)** GFP, CEP55 or CEP55 mutants were coupled to GFP dynabeads and incubated with MTs. Binding of MTs to CEP55 was assessed by Western blotting. **(C)** MTs were pulled down by ultracentrifugation and the concentration of CEP55 in pellet and supernatant was analyzed by Western-botting. The percentage of CEP55 in the pellet fraction was calculated. **(D)** CEP55 mutants were co-incubated with Rhodamine-labeled MTs (red) and analyzed by fluorescence microscopy. Shown are mean values + SD of three independent experiments. *p<0.5, **p<0.005, ***p<0.0001.

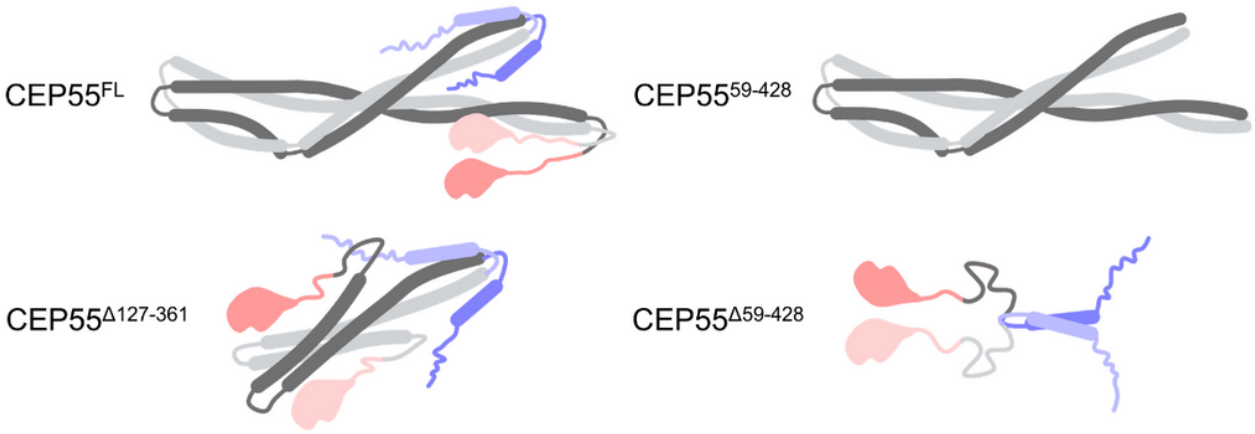

Figure 8

Alpha fold prediction of CEP55 and mutants. Full length CEP55 and the mutants $CEP55^{59-428}$, $CEP55^{D127-361}$ and $CEP55^{D59-428}$ are shown.

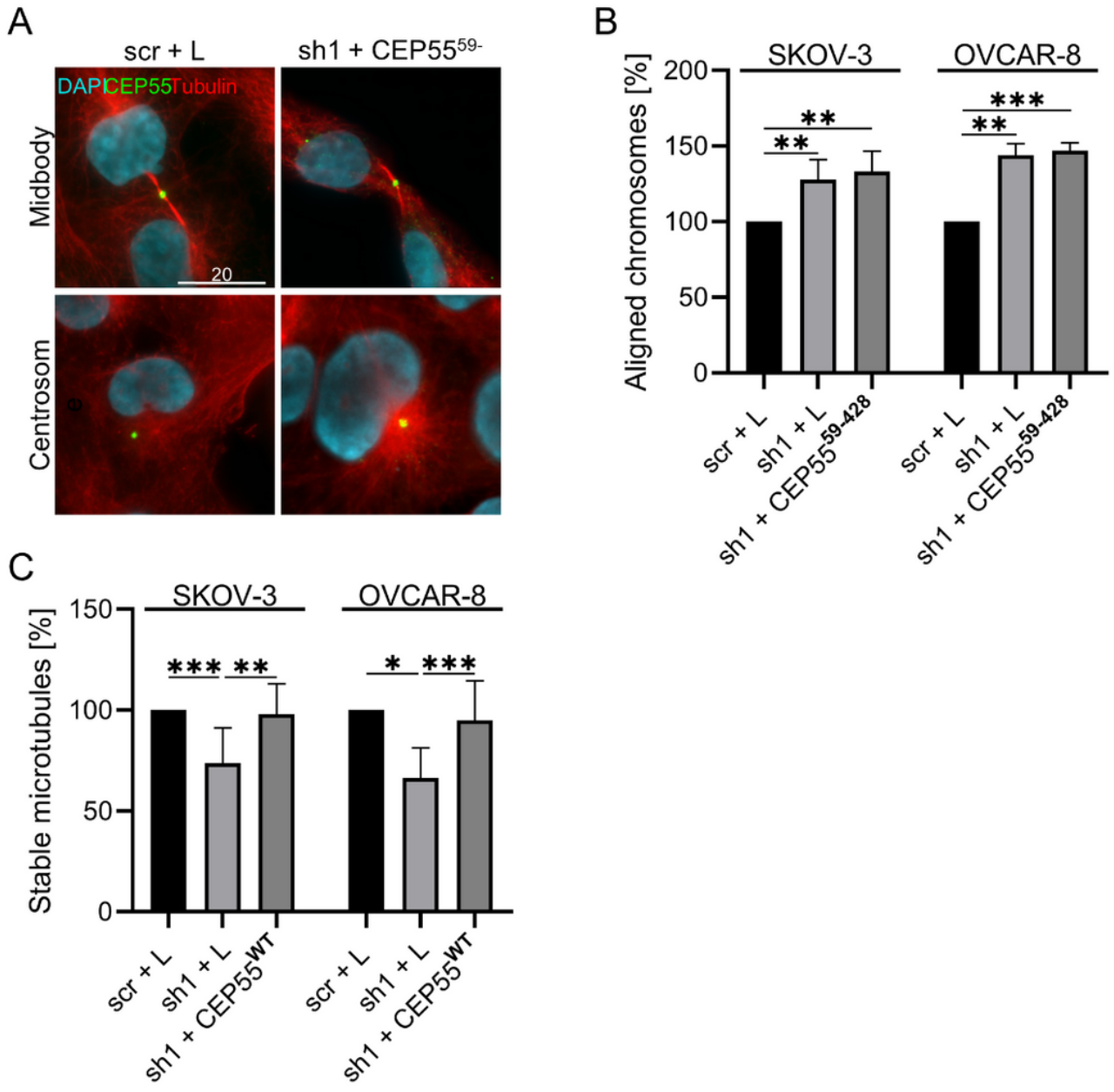

Figure 9

Re-expression of a CEP55 mutant with deficient MT-binding activity does not restore increased CIN of control cells. (A) Fixed cells were stained with antibodies against CEP55 (green) and MTs (red). **(B)** Metaphase cells were stained with Alexa-fluor568 coupled antibodies against b-tubulin and DAPI. The cells were grouped in cell populations with aligned end or not aligned chromosomes and counted. **(C)** Fixed interphase cells were stained with DAPI, the number of cells having micronuclei (indicated by arrows) were counted and the percentage of cells with micronuclei was calculated. **p<0.001, ***p<0.0001.

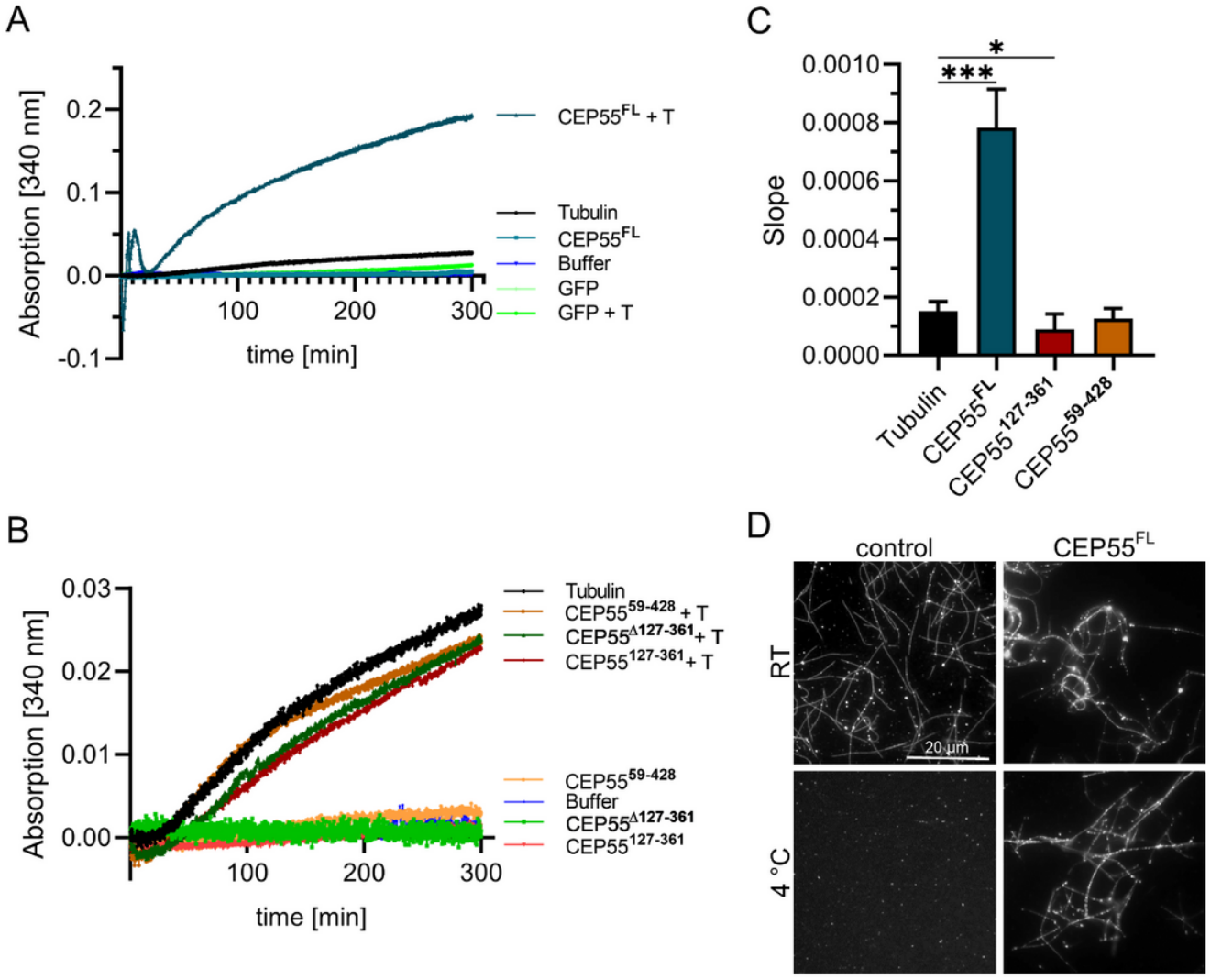

Figure 10

CEP55 increases MT-polymerization. Polymerization of non-labeled, non-stabilized MTs was assessed by a turbidity assay in presence and absence of **(A)** CEP55 o**r (B)** CEP55 mutants. In addition, all proteins in absence of MTs were measured as controls. **(C)** Mean values + SD of three independent experiments. *p<0.5, **p<0.005, ***p<0.0001. **(D)** Rhodamine labeled MTs were incubated at 4 °C/4 mM $CaCl_2$ in presence of GFP or GFP-CEP55.

Supplementary Files

This is a list of supplementary files associated with this preprint. Click to download.

- Supplemental.docx